An Experimental Study of Radar-Centric Transmission for Integrated Sensing and Communications

Murat Temiz, *Member, IEEE*, Colin Horne, Nial J. Peters, Matthew A. Ritchie, *Senior Member, IEEE*, and Christos Masouros, *Senior Member, IEEE*

***Abstract*— This study proposes a dual-function radar and communication (DFRC) system that utilizes radar transmission parameters as modulation indexes to transmit data to the users while performing radar sensing as its primary function. The proposed technique exploits index modulation (IM) using the center frequency of radar chirps, their bandwidths, and polarization states as indexes to modulate the communication data within each radar chirp. By utilizing the combination of these indexes, the proposed DFRC system can reach up to 17 Mb/s throughput, while observing a robust radar performance. Through our experimental study, we also reveal the trade-off between the radar sensing performance and communication data rate, depending on the radar waveform parameters selected in the DFRC system. This study also demonstrates the implementation of the proposed DFRC system and presents its real-time over-the-air experimental measurements. Consequently, the simulation results are verified by real-time over-the-air experiments, where ARESTOR, a high-speed signal processing and experimental radar platform, has been employed.**

***Index Terms*— Dual-function radar and communication (DFRC) systems, index modulation (IM), radar sensing, wireless communication.**

I. Introduction

RADAR and communication systems have been converging in the frequency spectrum owing to the growing number of civilian radar sensing applications and higher data rate demand of modern wireless communication systems with each passing day [1]. As a result, the frequency spectrum has been increasingly more congested, especially in the sub-10 GHz frequency bands that are attractive for both wireless communications and various radar applications. Consequently, researchers from academia and industry started focusing on the efficient and intelligent utilization of scarce frequency resources for both radar and communication systems. A promising solution to this problem is to enable both radar and communication systems on a single platform to use the same frequency resources. If two different waveforms are used for radar sensing and communications, each system will receive the waveform of the other as interference. Therefore, interference management, interference mitigation, or interference utilization techniques can be applied to negate to some degree the interference effects. Several dual-function radar and communication (DFRC) systems have been developed based on various techniques such as designing optimum waveforms and beamformers for communication and radar signals to reduce the interference between them [2], [3], predicting the radar interference and utilizing it for communications via optimized precoders [4] or mitigating the interference between radar and communication systems by advanced signal processing techniques [5], [6].

As an alternative to the above techniques, instead of transmitting separate radar and communication waveforms, several studies have concentrated on utilizing the same signals for both operations. The first category of such techniques termed *radar-centric* solutions [7], [8] operate by encoding communication data in the radar signals [9], [10], [11], while a separate family of techniques termed *communication-centric* aims to utilize communication signals, e.g., orthogonal frequency-division multiplexing (OFDM) waveforms, for radar sensing [12], [13], [14]. Moreover, some studies have focused on developing dual-function waveforms that are combinations of radar and communication waveforms [15], [16], [17], the parameters of which can be adjusted to deliver a desired trade-off between radar and communication subsystems, depending on the application. In this study, we implement and demonstrate a *radar-centric* method that aims to enable communication functions in short-range radar systems by utilizing index modulation (IM) within frequency-modulated continuous-wave (FMCW) radar chirps. Accordingly, this study puts forward a radar-centric approach for DFRC systems, where the primary function is radar sensing while transmitting data to the communication users.

The concept of IM has been recently seen as a promising solution for next-generation wireless networks since it can utilize various waveform features as modulation indexes at the same time, unlike the conventional modulation techniques that generally make use of amplitude, frequency, or phase variations to modulate the data [18]. For instance, selections of transmit antennas, subcarriers, time slots, spreading codes or other signal features can be employed as indexes [18], [19].

Manuscript received 18 September 2022; revised 15 December 2022; accepted 30 December 2022. This work was supported by the Defense and Security Accelerator (DASA), and by the UK EPSRC under grant number EP/S035362/1. *(Corresponding author: Murat Temiz.)*

The authors are with the Department of Electronic and Electrical Engineering, University College London, London WC1E 7JE, U.K. (e-mail: m.temiz@ucl.ac.uk; colin.horne.14@ucl.ac.uk; nial.peters@ucl.ac.uk; m.ritchie@ucl.ac.uk; c.masouros@ucl.ac.uk).

Color versions of one or more figures in this article are available at https://doi.org/10.1109/TMTT.2023.3234309.

Digital Object Identifier 10.1109/TMTT.2023.3234309

Moreover, by utilizing various indexes at the same time, large constellation sizes can be obtained to modulate a large number of bits into each symbol. This results in more spectral and energy efficient communication as long as the complexity of the demodulation process at the receiver is acceptable and practical such that it does not require high computational resources and energy for demodulation.

Since IM does not require special waveform types and can be performed without significantly changing the signals, IM has been recently considered to transmit data within radar waveforms [20], [21], [22], [23], [24], [25], [26], [27], [28], [29]. One of the first attempts to utilize radar waveform features as indexes to deliver data was in [20], where the radar system selects the antennas out of all antenna elements available in the array and assigns orthogonal radar waveforms to them in order to embed data into radar pulses, achieving megabits per second data rates while performing radar sensing as the primary function. Another study in [21] proposed multicarrier agile joint radar-communication (MAJoRCom) system which combines antenna selection and carrier frequency selection of radar waveforms and utilizes these combinations to modulate data. Moreover, they also investigated low-complexity precoder design and code-book design to reduce the complexity and enhance its performance. Şahin et al. [22] considered modulated circularly-shifted chirps (CSC), where the communication data is encoded via indexes and phase shift keying (PSK) in the CSC that is a multicarrier radar waveform. These studies [20], [21], [22] considered pulsed Doppler radar waveforms, such as linear frequency modulation (LFM) signals, that are mainly used for long-range and military radar applications. On the other hand, the study in [23] proposes a method that works with FMCW, a technique mainly used in short-range radars. The method proposed in [23] makes use of the active antenna index and carrier frequency selection of the FMCW radar to modulate data. Since this utilizes continuous waveforms for radar and communication, this method can be used in self-driving vehicles or other short-range sensing applications. Moreover, embedding communication data in frequency-hopped multiple-input multiple-output (FH-MIMO) radar systems through IM has been also considered to develop integrated sensing and communication systems [27], [28], [29], and these FH-MIMO DFRC studies have been recently reviewed in [30]. For instance, the communication data may be embedded into radar waveforms in an FH-MIMO radar system using various signaling strategies such as antenna selection, quadrature amplitude modulation (QAM), PSK modulation or carrier frequency selection [29]. On the other hand, OFDM waveforms were also considered with IM such as in [26], where authors proposed a DFRC scheme that conveys data by selecting the subcarrier indexes of the OFDM signals in addition to the data conveyed through the OFDM signals themselves while also performing radar sensing.

In the aforementioned IM-based DFRC studies, it is generally assumed that the channel state information (CSI) is known by the communication receivers, therefore it is possible to utilize multiple antennas and phase diversity as indexes of modulation as the waveforms transmitted by each antenna element and phase information can be decoded using the precise CSI. However, the CSI may not be accurately acquired due to the nature of radar waveforms, therefore such ideas are difficult to implement in real-time applications where the channel varies rapidly making CSI estimation challenging using radar waveforms. Precise CSI information is especially required in these methods when they need to estimate the phase and antenna index at the receiver. Moreover, in a moving transmitter and receiver scenario with real-world clutter and multipath the estimation of the exact transmit element will be very challenging. Therefore, in this study, we explore the new use of polarization of the transmitted radar waveform as a parameter, which is easier to estimate at the communications receiver node. The signals received in different polarizations can be distinguished by utilizing the polarization diversity at the receiver without requiring CSI.

This study proposes a radar-centric approach for enabling communication functionality without significantly affecting the radar performance and also maintaining a low probability of intercept for the radar system by varying the center frequency and waveform bandwidth. To this end, parameters of the transmitted radar chirps are utilized as indexes to obtain a large constellation diagram to transmit the communication data at relatively high data rates. Utilizing vertical (V-pol) and horizontal polarizations (H-pol) for radar sensing also enables the radar to capture more information about the targets since some target features may be better acquired in one specific polarization and a dual-polarized radar may also provide a higher signal-to-noise ratio (SNR) [31]. This also mitigates the impact of the interference from other RF devices operating in the same frequency band as the interference is likely to happen in only one of the polarizations [32]. The University College London (UCL) ARESTOR platform [33] was used as the experimental platform on which to validate the proposed DFRC concept. This system is capable of operating as an active radar, a passive radar and an electronic surveillance (ES) system. A bespoke waveform design architecture was implemented for this work allowing the transmission of the predefined codebook of waveforms to enable joint radar and communications. This capability was validated in both lab-based loop back experiments and field trials with moving targets.

Contributions

The contributions of this study are summarized as follows.

1) This study proposes a novel IM-based DFRC architecture that exploits dual-polarized antennas. In previous studies, polarization is not considered an index.
2) This study proposes a low hardware complexity method that requires a maximum of two radio frequency (RF) transmit chains and two RF receive chains for each receiver to perform both radar sensing and communication, by utilizing two different polarizations and radar waveform parameters. This results in simplified transmitter and receiver architectures compared to prior index-modulation DFRC literature.
3) The proposed DFRC architecture does not require a precise channel estimation in line-of-sight (LOS) channels

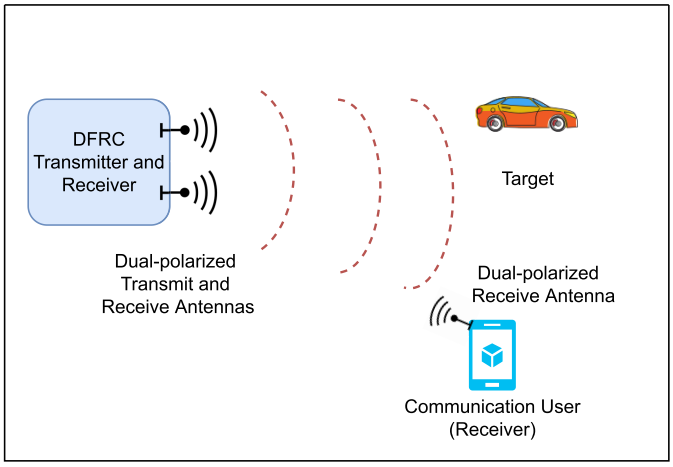

Fig. 1. IM-based FMCW DFRC system.

since it does not need the phase information of the transmitted signals and antenna diversity is provided by the polarization, accordingly the chirps can be demodulated without CSI at the communication receiver.

4) This study experimentally shows the trade-offs between the radar sensing performance and communication data rate depending on the radar waveform parameters. The trade-off is obtained by varying the pulse repetition interval (PRI). A long PRI results in a greater radar integration gain, while a short PRI favors a higher communication rate. To the best knowledge of the authors, this is the first study in the literature to experimentally demonstrate the trade-offs, over-the-air, between the radar and communication performances in an index-modulated DFRC system.
5) A technique for compensating for changes in radar range cell extent caused by signal bandwidth-based index coding of the communications data is proposed and implemented on the experimental radar data.

II. System Model

The proposed radar and communication system utilizes the features of FMCW chirps as indexes to deliver communication data while performing radar sensing as the primary function of the platform as shown in Fig. 1. The waveform carrier frequency (f_c), bandwidth (B), and polarization of the transmitted radar chirps are chosen as indexes to modulate the communication data.

A. FMCW Signal Model and IM

In this section, we will first mathematically define the FMCW chirps and then give the details of the IM technique employed in the proposed DFRC model. An FMCW chirp is given by the following equation:

$$u(t) = Ae^{-j\pi\left(2f_c t + kt^2\right)}, \quad t \in [0, T_c] \tag{1}$$

where $A(t)$, f_c, and T_c denote the amplitude, carrier frequency, and sweep duration of a chirp, respectively, and $k = B/T_c$ denotes the slope of the chirp where B is the bandwidth of the chirp. Moreover, the generated chirps are transmitted either by V-pol, H-pol or both (V- and H-pols) antennas ($\{V, H, VH\}$) such that amplitude $A = 0$ when there is no transmission in that polarization. Furthermore, it is also possible to simultaneously transmit two different chirps in V- and H-pols. Accordingly, the transmitted nth baseband DFRC signal consisting of chirps transmitted in V- and H-pols and with modulation indexes is given by the following equation:

$$X_n = u_n^V(t) + u_n^H(t) = A^V e^{-j\pi\left(2f_c^V t + B^V/T_c t^2\right)} + A^H e^{-j\pi\left(2f_c^H t + B^H/T_c t^2\right)} \tag{2}$$

where $t \in [0, T_c]$, and superscript V and H denote the polarizations of the modulation indexes A, f_c, and B. Moreover, $A^V \in \{0, 1\}$ and $A^H \in \{0, 1\}$ denote if there is a chirp transmitted in the corresponding polarization during the nth transmission, resulting in the polarization index $p_n = \{V, H, VH\}$. The bandwidth, carrier center frequency, and polarization, of the FMCW chirps are utilized as indexes for data modulation within radar chirps. Let us assume that carrier frequency f_c is varied by Δ_f steps between $f_{(\min)}$ and $f_{(\max)}$ as follows:

$$f_{(\min)} \le f_{(\min)} + k\Delta_f \le f_{(\max)} \tag{3}$$

where $k = 0, 1, \ldots, K-1$ is the index of the center frequency and K denotes the number of center frequency indexes, and hence $f_c = f_{(\min)} + k\Delta_f$. In a similar way, the set of bandwidth options for the FMCW chirps can be defined as follows:

$$B_{(\min)} \le B_{(\min)} + l\Delta_B \le B_{(\max)} \tag{4}$$

where $B_{(\min)}$, $B_{(\max)}$, Δ_B and $l = 0, 1, \ldots, L-1$ denote the minimum bandwidth, maximum bandwidth, bandwidth spacing, and bandwidth index, respectively. Moreover, L denotes the number of bandwidth indexes and bandwidth of the chirp is $B = B_{(\min)} + l\Delta_B$. Only three polarization states are considered, namely only vertical, only horizontal or both, therefore, the number of polarization indexes can be given by $P = 3$.

The proposed method provides a low hardware complexity DFRC architecture as it does not require multiple antennas and precise channel estimation since the phase information of the signals is not used for communication. Consequently, only one dual-polarized antenna is sufficient to transmit waveforms for both radar and communication functions. Two different transmitter/receiver architectures are proposed in this study depending on the utilization of the polarization index.

B. Radar Signal Processing and Target Detection

The radar signals reflected from the targets are processed via standard FMCW radar processing techniques. The general principles and applications of FMCW radar are described in [34] and [35]. The processing involves mixing the return signal with a replica of the transmitted chirp signal, a process known as de-ramping. The result of de-ramping is a "beat" signal, the frequency of which represents the range of the target the return has been reflected from. Target ranges can therefore be determined by spectral analysis of the beat signal. Traditionally the de-ramping process has been achieved in

the analog domain allowing the relatively low-frequency beat signal to be subsequently digitized by low-speed analog to digital converters for further processing. In the ARESTOR implementation of FMCW radar the target return signal and the original transmitted signal are directly digitized at RF and mixed down to baseband digitally. The mixing of the two signals is then also completed digitally to produce the beat signal. The decimation of the resulting signal is carried out to reduce the sample rate to a value consistent with the spectral occupancy of the practical range of beat signals. The spectral analysis is carried out in the ARESTOR hardware which can produce real-time output to a user display. Details of the ARESTOR FMCW radar implementation can be found in [36].

An important negative feature of the proposed joint radar and communication waveforms is introduced by the variation of FMCW chirp bandwidth, which creates an accompanying variation of radar range cell size. This is unusual in FMCW implementations. This behavior provides an additional challenge in target range determination as the range cell extent of the de-ramped spectrally processed data varies with bandwidth. A method to compensate for the impact of changing bandwidth on radar sensing is proposed and implemented. This modified processing involves scaling the fast Fourier transform (FFT) length in the spectral analysis processing based on the bandwidth of chirp signal transmitted on the specific interval such that the range extent represented by the FFT bins is equal across all bandwidths. The range cell extent r for a given bandwidth B is given by the following equation:

$$r(B) = \frac{cS_{\text{dec}}T_c}{2BN_{\text{FFT}}} \tag{5}$$

where c, S_{dec}, and N_{FFT} denote the speed of light, the decimated complex sample rate, and the FFT size, respectively. It can be seen that the range cell extent decreases with increasing bandwidth for the remaining parameters being constant.

Defining $N_{\text{FFT}_{\text{min}}}$ as the FFT length applied to the signal with the highest available bandwidth B_{max} and $r(B_{\text{max}})$ as the related range cell extent, then the FFT length N_{FFT_B} for alternative bandwidths which achieve equal range cell extent is

$$N_{\text{FFT}_B} = \frac{r(B)N_{\text{FFT}_{\text{min}}}}{r(B_{\text{max}})}. \tag{6}$$

For fixed values of parameters other than bandwidth this simplifies to

$$N_{\text{FFT}_B} = \frac{B_{\text{max}}N_{\text{FFT}_{\text{min}}}}{B}. \tag{7}$$

The use of variable FFT lengths as described enables a single-step solution to implementing the required spectral analysis and correcting the resulting target range determination, rather than using interpolation techniques to map the fixed length FFT results to the physical range. This additional processing uses data directly derived from the de-ramp processing and is implemented in software on a computer rather than in the ARESTOR hardware platform. Results generated by this modified FMCW processing can be seen in Section V.

The variation in bandwidth and center frequency of the transmitted signal also makes conventional Doppler processing of the radar returns for target velocity estimation impossible. In this work, we have not considered the challenge of how the returns might be further processed to provide target Doppler information and its viability remains an open question.

Due to modulating data within FMCW chirps, the maximum unambiguous range of the radar and communication throughput are now coupled. A higher pulse repetition frequency (PRF) will give a higher data rate but also limit the maximum permissible duration of each chirp. For an FMCW radar receiver with a given bandwidth, reducing the chirp duration also reduces the maximum unambiguous range. If long-range radar sensing is required, this may conflict with simultaneous high data throughput. This is an example trade off decision that would need to be made when operating the joint index-modulated radar-communications system in real scenarios. This trade-off between radar sensing performance and communication throughput is also shown for the proposed DFRC system.

As radar performance metrics, the SNR of the radar returns and Cramér–Rao lower bound (CRLB) on the range estimation are used in order to investigate the trade-off between the radar and communication performances. For simulations and field-trial measurements, the SNR is defined as $\text{SNR} = p_{\text{sig}}/p_{\text{noise}}$, where p_{sig} and p_{noise} denote the signal power and noise power per channel, respectively. Moreover, different SNR levels are obtained while processing the baseband data by measuring the average received signal power p_{sig} during chirp transmissions in the time domain and artificially adding a corresponding additive white Gaussian noise (AWGN) to baseband signals in order to obtain the desired SNR levels.

C. Cramér–Rao Lower Bound

CRLB determines the lower bound on estimator error variance for unbiased estimators of a deterministic unknown parameter. Therefore, a lower CRLB on range indicates a better range estimation, i.e., lower estimation error. CRLB on range defines the theoretical lower bound of range estimation errors in radar systems and it is frequently used to evaluate the performance of radar sensing systems [37]. It is mainly dependent on the waveform bandwidth, waveform type, SNR, and chirp duration, making it a suitable radar performance metric for this study since the waveform bandwidth and center frequency vary chirp to chirp as a result of modulating the communication data on the chirps. An analytical expression to calculate CRLB on the range for an FMCW radar is given by [38]

$$\text{CRLB}_r = \frac{3c_0^2}{4\pi^2\rho N_s B^2} \tag{8}$$

where ρ, $c_0 \approx 3 \times 10^8$ m/s, $N_s = 500$ denote the SNR of the radar returns, the speed of the waves (i.e., light speed), and number of samples taken during the observation, respectively [38]. This equation indicates that the range estimation accuracy improves as the chirp bandwidth, SNR and number of samples increase. It is worth noting that the unit of the

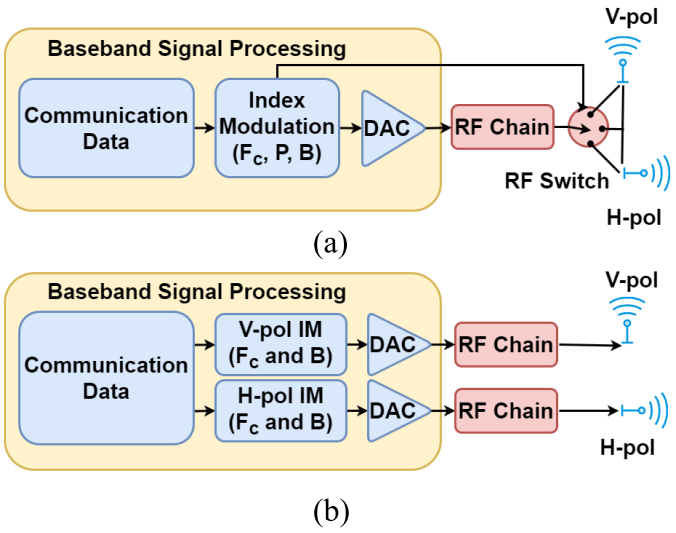

Fig. 2. IM-based DFRC transmitter architectures: (a) single digital and RF channel transmitter and (b) dual digital and RF channels model.

CRLB on the range is m^2 since it indicates the lower bound on the estimator error variance (σ^2) of range estimations.

D. Radar and Communication Transmitter

The radar node modulates the radar chirps using the IM technique (polarization, center frequency and bandwidth) to transmit data to communications users while performing sensing using the same chirps. In addition to a dual-polarized transmit antenna, the radar node also has a dual-polarized radar receive antenna allowing simultaneous transmit and receive. For each FMCW chirp, radar waveform $T_x(t)$ is transmitted either in V-pol or in H-pol or simultaneously in both polarizations. The radar target detection is performed by processing the radar returns from the target while the communication users can decode the received radar signals by determining the indexes of each transmitted FMCW chirps.

We consider two different transmitter architectures employing either one digital and RF channel or two channels as shown in Fig. 2. Therefore, the hardware complexity can be reduced if necessary at the expense of communication data rate as this will be shown in the numerical results. Fig. 2(a) illustrates that a single digital block and RF chain are used to serve both polarizations using an RF switch. In this case, only one waveform can be transmitted in either H- or V-pols or in both polarizations during one chirp duration. In the second architecture given by Fig. 2(b), each antenna is connected to independent digital blocks and an RF chain. Accordingly, during a chirp duration, independent waveforms can be transmitted in H- and V-pols. This enables higher data rates compared to the first architecture at the cost of additional hardware and hence consumes more power. Simultaneous transmission of different waveforms in H- and V-pols has the potential to severely impact radar performance since any cross-polarization scattering will result in both waveforms being detected by the receiver. For an FMCW radar, this could result in false targets being created due to the scattered V-pol waveform being deramped using the H-pol waveform or vice versa. For a single-polarization radar receiver, for example, H-pol, this can be addressed by only transmitting V-pol waveforms whose instantaneous frequency is less than that of the transmitted H-pol waveform. In this way, any signal due to cross-polarization scattering will deramp to a negative frequency and can be ignored. This strategy comes at the cost of a reduced number of possible symbols, and therefore reduced communications throughput. For a dual-polarised radar receiver, the false targets will only appear in one polarization (in the other they map to negative frequencies and can be easily ignored), therefore they may be identified and discarded without a loss in communications performance.

The radar receiver part is not shown in Fig. 2. A standard dual-polarized receiver can be used with some additional signal processing stages to mitigate the impact of the varying chirp bandwidth and center frequency as explained in Section II-B. The first transmitter architecture transmits a single chirp in each time block in either V, H, or both in VH polarizations. Therefore, only a single digital-to-analog converter and a single RF transmitter chain are required. This enables a low-hardware complexity radar and communication architecture. The second transmitter architecture transmits two independent chirps in V and H pols, therefore, this requires two DACs and RF chains. However, it achieves higher throughput. Considering that L bandwidth and K center frequency options are available to select to modulate the data, then the number of bits that can be transmitted in each chirp duration by the first transmitter architecture with three possible polarization states (V, H, and VH) is given by the following equation:

$$N_{\text{bits}} = \lfloor \log_2(3\text{KL}) \rfloor \tag{9}$$

where $\lfloor . \rfloor$ defines the floor function. On the other hand, the number of bits transmitted by the second architecture, where independent chirps are transmitted by H- and V-polarized antennas simultaneously, is given by the following equation:

$$N_{\text{bits}} = \lfloor \log_2(KL)^2 \rfloor = \lfloor 2\log_2(\text{KL}) \rfloor. \tag{10}$$

Moreover, the communication throughput is a function of the number of bits correctly transmitted per second, accordingly the throughput of the DFRC system is given by the following equation:

$$R_{\text{com}} = \frac{1}{T_c} N_{\text{bits}} (1 - \gamma) \tag{11}$$

where T_c and γ denote the chirp duration and symbol error rate (SER), respectively. SER is affected by the SNR, Δ_f, Δ_B, and the interference between the two polarizations.

E. Comparison With Previous IM-Based DFRC Studies

In comparison with previous radar-centric DFRC studies [20], [21], [22], [23], [24], [25], [26], [27], [28], [29], this study presents a reduced hardware complexity method such that it does not need multiple antennas and multiple analog and digital processing chains. It only needs a dual-polarized antenna and one or two analog or digital processing chains. Moreover, it does not require precise CSI

TABLE I
COMPARISON OF IM-BASED DFRC STUDIES

Study	[21]	[23]	[25]	[28]	This study
Antennas	antenna array	antenna array	antenna array	antenna array	dual-polarized single antenna
IM Indexes	carrier frequency antenna selection	phase modulation antenna selection carrier frequency	phase modulation antenna selection	phase modulation sub-band selection antenna selection	carrier frequency chirp bandwidth polarization state
Channel Estimation	required	required	required	required	not required
Notes	Theoretical	Theoretical	Theoretical & Experimental	Theoretical	Theoretical & Experimental

as it utilizes polarization diversity instead of antenna diversity as an index and avoids using phase modulation. Furthermore, it can still achieve desirable data rates in comparison with other radar-centric DFRC methods recently published, as shown in Section V. This study also presented the real-world implementation of the proposed radar-centric DFRC method and over-the-air experimental measurements to demonstrate its communication and radar sensing performance. As a summary, Table I presents an overall comparison of this study to the related IM-based DFRC studies published in the literature.

III. COMMUNICATION RECEIVER ARCHITECTURE

The RF signals received by V-pol and H-pol communication antennas are directly digitized by the high-speed analog-to-digital converters (ADCs) of ARESTOR. After direct RF digitization, down-conversion is digitally performed and then digital signal processing is performed to detect the communication symbols. However, it is also possible to use conventional analog down-conversion blocks to obtain the baseband signals.

The wideband signals received in V- and H-pols at the communication receiver during the nth transmission can be given by the following equation:

$$S_n^V(t) = u_n^V(t) * h^V(t) + u_n^H(t) * h^{\mathrm{HV}}(t) + n^V(t) \quad (12)$$

$$S_n^H(t) = u_n^H(t) * h^H(t) + u_n^V(t) * h^{\mathrm{VH}}(t) + n^H(t) \quad (13)$$

where $*$ expresses the convolution operation, $u_n^V(t)$ and $u_n^H(t)$ denote the chirps transmitted in V- and H-pols given by (2). Moreover, $h^V(t)$ and $h^H(t)$ denote the channels of V and H polarizations, respectively, between the radar transmitter and communication receiver, and $h^{\mathrm{HV}}(t)$ and $h^{\mathrm{VH}}(t)$ denote the cross-polarization channels between the V- and H-pols. Moreover, $n^V(t)$ and $n^H(t)$ denote the complex-valued AWGN in the V- and H-pols channels with zero mean and noise variance p_n as $\mathcal{CN}(0, p_n)$.

A. Single Channel Baseband Receiver

The first receiver architecture considered is a two-stage receiver that first determines the polarization of the received chirps and then estimates the carrier center frequency and bandwidth of the chirps by utilizing a single maximum likelihood estimator as shown in Fig. 3(a). This approach provides a low-computational complexity since the maximum likelihood estimator is only performed in a single polarization and the

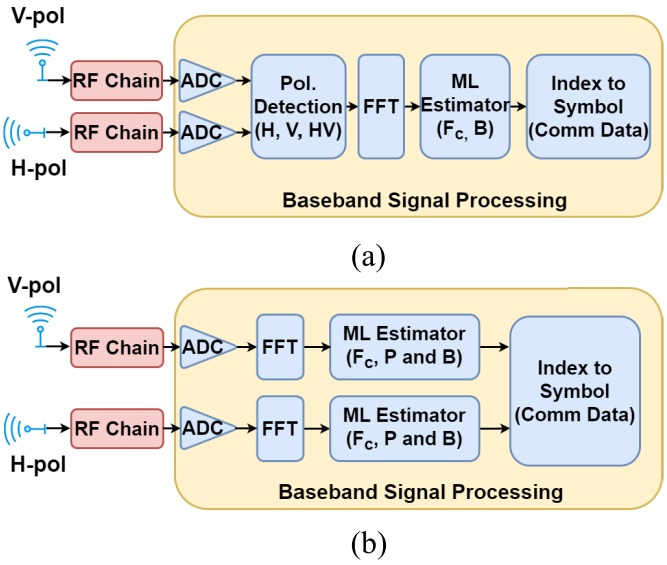

Fig. 3. IM-based DFRC receiver architectures: (a) polarization detection and single maximum likelihood estimator and (b) two parallel maximum likelihood estimators.

number of possible symbol combinations in this maximum likelihood estimator is KL. Moreover, it requires only one FFT after determining the polarization of the received signals. The disadvantage of this method is that it cannot be used when independent chirps are transmitted simultaneously in V and H pols. Furthermore, it is more prone to noise and interference between the polarizations since the detection of the polarization is performed by comparing the power of received signals in V- and H-pols to a power threshold. It is difficult to determine an optimum power threshold since it should be determined by taking into account both cross-polarization interference and noise, both of which may vary over time.

Fig. 3(a) illustrates the single maximum likelihood receiver architecture, where the received signals from both polarization channels are first processed by the RF chains and converted into an intermediate carrier frequency. The detection of the transmitted data is performed in two stages in order to reduce the complexity. In the first stage, the polarization of the received signals is detected by comparing them to the noise level. This stage will return the polarization state of the received nth chirp as $\hat{p}_n$.

Let us assume that the ratio of the polarization leakage amplitudes between H- and V-pols is denoted by α_{pol}, then the threshold of the polarization detector, T_{pol}, is given by the

following equation:

$$T_{\text{pol}} = \sigma_n^2 + p_{\text{sig}}/\beta + \alpha_{\text{pol}}^2 \tag{14}$$

where σ_n^2 denotes the noise variance and β is the ratio that needs to be optimally selected with regard to the polarization leakage α_{pol} and noise variance σ_n^2. This is because the received signal power is the combination of the received signals from both polarizations and noise, and hence the threshold should be adjusted with regard to the polarization leakage. While determining the threshold T_{pol}, the first pulse transmitted in either V-pol or H-pol can be used to estimate p_{sig} to improve the stability of polarization detection. After estimating the polarization of the received signal as $\hat{p}_n \in \{V, H, VH\}$, the received chirp $S_n(t) \in \{S_n^V(t),\ S_n^H(t)\}$ in either H-pol or V-pol during chirp duration T_c is converted into the frequency domain using the Fourier transform as follows:

$$W_n = \int_{-\infty}^{\infty} S_n(t) e^{-j2\pi ft} dt \tag{15}$$

where $0 \leq t \leq T_c$ for each chirp. The FFT method is used to take the Fourier transform of the received signals after down-conversion. After FFT processing, the received signals are normalized before detecting the bandwidth and center frequency.

In the second stage, the bandwidth and the center frequency of the received chirps are estimated by a maximum likelihood estimator that compares this sampled data to the codebook that contains all possible chirps with bandwidth and center frequency combinations. This is expressed as follows:

$$\underset{(\hat{k}_n, \hat{l}_n)}{\arg\min} \quad \|W_n - \mathcal{F}\|_2 \tag{16}$$

where $\mathcal{F} = \{W_{(1,1)}, \ldots, W_{(k,l)}, \ldots, W_{(K,L)}\}$ denotes the set of chirps (i.e., code-book) with all possible bandwidth and center frequency combinations, and $||\cdot||_2$ indicates the L_2 norm operation. Moreover, W_n denotes the nth received radar chirp in the frequency domain and $(\hat{k}_n, \hat{l}_n)$ denotes the estimated center frequency and bandwidth indexes of the nth radar chirp. Including the estimated polarization $(\hat{p}_n)$, the indexes of the detected symbol can be given as $(\hat{p}_n, \hat{k}_n, \hat{l}_n)$ and this can be de-mapped to the communication data. This receiver architecture can be only used by the first receiver architecture as it assumes that either the chirp is transmitted in one polarization or the same chirp is transmitted in both polarizations.

B. Dual Channel Baseband Receiver

In the second approach, two maximum likelihood estimators are performed in parallel as shown in Fig. 3(b), each estimator is connected to one of the dual-polarized antenna channels (V- and H-pols antennas). This method can be used with both transmitter architectures as the chirps simultaneously transmitted in both polarizations can be estimated. Each maximum likelihood estimator searches for the correct symbol in the codebook, i.e., center frequency and bandwidth combination of the chirps received in V- and H-pols. Note that this method requires that the FFT must be performed in both polarizations before the maximum likelihood estimators while in the previous method, the FFT needs to be performed in either the V-pol or H-pol after estimating the polarization state of the received chirp.

The Fourier transform is performed on the received nth chirps in V- and H-pols to convert them into frequency domain samples as follows:

$$W_n^V = \int_{-\infty}^{\infty} S_n^V(t) e^{-j2\pi ft} dt \tag{17}$$

$$W_n^H = \int_{-\infty}^{\infty} S_n^H(t) e^{-j2\pi ft} dt \tag{18}$$

where superscript V and H denote the polarizations. In the second receiver architecture, illustrated by Fig. 3(b), two maximum likelihood (ML) estimators concurrently operate to estimate the transmitted communication symbols. Note that in one of the polarizations, there may not be a transmitted signal in the case of using the first transmitter architecture as it may transmit in either of the polarization. Therefore, the set of waveform options (i.e., codebook) should also include a no-transmission case as $\mathcal{F} = \{W_{(0,0)}, W_{(1,1)}, \ldots, W_{(k,l)}, \ldots, W_{(K,L)}\}$ where $W_{(0,0)}$ denotes that there is no chirp transmission. Two ML estimators can concurrently operate to detect the symbols transmitted in V and H polarizations as follows:

$$\underset{(\hat{k}_n^V, \hat{l}_n^V)}{\arg\min} \quad ||W_n^V - \mathcal{F}||_2 \tag{19}$$

$$\underset{(\hat{k}_n^H, \hat{l}_n^H)}{\arg\min} \quad ||W_n^H - \mathcal{F}||_2 \tag{20}$$

and the ML estimators return the estimated indexes $(\hat{k}_n^V, \hat{l}_n^V)$ and $(\hat{k}_n^H, \hat{l}_n^H)$ for the signals received in V- and H-pols, respectively. The computational complexity of each ML estimator is related to the number of possible symbols that can be transmitted in each polarization, i.e., $KL + 1$. This receiver architecture can demodulate the chirps transmitted by both transmitter architectures shown in Fig. 2(a) and (b). After estimating the indexes of the chirps using the aforementioned single or dual baseband channel receivers, these indexes are de-mapped to the communication symbols at the receiver.

IV. RF Sensor Hardware Platform - ARESTOR and Experimental Setup

This section explains the RF sensor platform used in experiments and gives the details of the over-the-air experimental setup.

A. RF Sensor Hardware Platform - ARESTOR

The hardware used to experimentally validate this dual-function concept was the UCL ARESTOR platform [33]. ARESTOR is a xilinx RF system on chip (RFSoC) [39] based system that uses the Xilinx ZCU111 development board [40] as its core, Fig. 4.

The RFSoC is a conventional field programmable gate array (FPGA) providing a substantial programmable logic (PL) fabric, and in addition the device includes high-speed

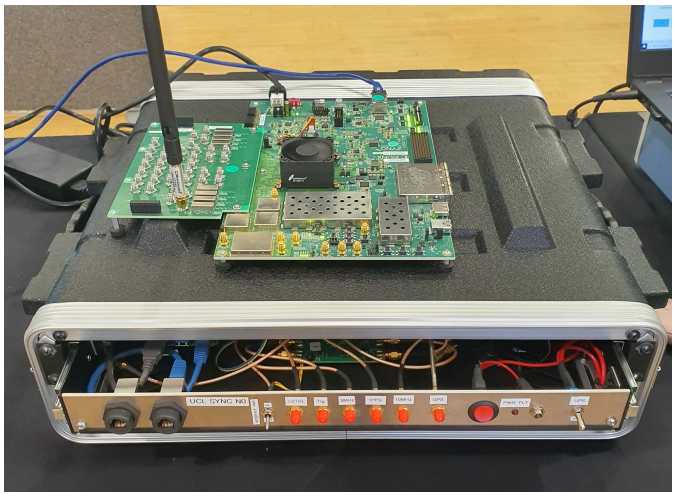

Fig. 4. UCL ARESTOR System based on the Xilinx RFSoC ZCU111 Evaluation Board.

TABLE II
CHARACTERISTICS OF GENERATION 1 RFSOC DEVICE

No of DAC / ADC Bits	14 / 12-bit
No of channels DAC / ADC	8 / 8
ADC Sample Rate	4.096 GSPS
DAC Sample Rate	6.554 GSPS
System Logic Cells (K)	930
System Memory (MB)	60.5
DSP Slices	4272
Processors	Arm Cortex-A53 + Arm Cortex-R5

ADCs and digital-to-analog converters (DACs). The ZCU111 development board contains a generation 1 RFSoC device with 8 ADCs operating in excess of 4 G-samples/s, and 8 DACs operating in excess of 6 G-samples/s. Later generation devices provide expanded options including higher sample rates and/or larger numbers of ADCs and DACs. The characteristics of the RFSoC device used on the ZCU111 are shown in Table II. In addition to the system memory present on the RFSoC, the ZCU111 also provides two blocks of 4 GB DDR memory attached to the PL and processing system (PS) of the RFSoC, respectively. In ARESTOR, the PS DDR has been upgraded to 32 GB.

The ARESTOR platform has been developed at UCL to provide a flexible, highly configurable RF sensor capable of operating in multiple sensing modalities. These modalities might be operated serially by reconfiguring the device as necessary on-the-fly, or given sufficient resources within the device multiple modalities can be operated in parallel. As an example, ARESTOR can support FMCW active radar concurrently with a passive radar implementation in different frequency bands with the use of an RF front end [36].

In addition to the evaluation hardware system the ARESTOR platform consists of an ecosystem which provides in-built tools which automatically configure and build the chosen design elements to form the final personality of the system. This relies heavily on a series of Python scripts which interact with the Xilinx development tools. The ecosystem includes a number of standard modules which may be connected together to form the desired system such as FMCW active radar blocks

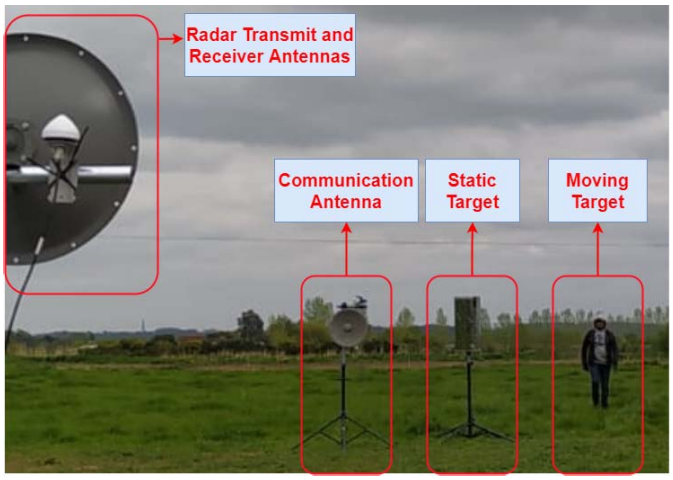

Fig. 5. Field trials of the proposed architecture.

which implement the signal de-ramping process, decimation blocks which reduce the data throughput and passive radar processing components, amongst others.

B. Experimental Set-Up

For this application, we use two ARESTOR platforms, one to implement the FMCW active radar transmitter and receiver, which is also communications source, and a second as the communications receiver. Although the FMCW radar node design was available from previous development the existing design did not allow for changes in the signal parameters over the course of a data capture, therefore further development was required to enable chirp to chirp modification of the signal parameters necessary for packaging the communications payload. Another area where the standard FMCW processing was not directly applicable is in the mapping of the de-ramped return signal to the physical range of the target. The range resolution and range cell extent are dependent on the bandwidth of the transmitted signal, which in this scenario is in turn dependent on the symbol being transmitted, therefore the range cell size will vary from PRI to PRI. This effect can be compensated for as described in Section II-B. The standard FMCW radar processing operates in real-time on the ARESTOR platform and can provide a real-time display of the scene. However, the radar range correction processing is currently implemented off-line, as is the communications receiver.

The measurement setup is shown in Fig. 5, where the dual-polarized radar transmits antenna, communication receive antenna, and static and moving targets are shown. The moving target was walking toward the radar and away from the radar during measurements. Two ARESTOR platforms, shown in Fig. 4, were used in measurements, the first one was used as a radar node to perform radar sensing and transmit communication data, therefore, connected to two dual-polarized antennas (radar and communication transmit antenna and radar receive antenna), and the second ARESTOR platform was used as the communication receiver, connected to the dual-polarized communication receive antenna. During measurements, various radar waveform parameters are tested and their impact on

TABLE III

NUMBER BITS TRANSMITTED PER RADAR CHIRP FOR EXAMPLE BANDWIDTH AND CENTER FREQUENCY SEPARATIONS IN 2.4 GHz ISM BAND

ΔB	Δf	RF Chain	N_{cons}	N_{bits}
5 MHz	5 MHz	Dual	30^2	9 bits
2 MHz	2 MHz	Dual	126^2	13 bits
2 MHz	1 MHz	Dual	245^2	15 bits
1 MHz	1 MHz	Dual	426^2	17 bits
5 MHz	5 MHz	Single	$3 * 30$	6 bits
2 MHz	2 MHz	Single	$3 * 126$	8 bits
2 MHz	1 MHz	Single	$3 * 245$	9 bits
1 MHz	1 MHz	Single	$3 * 426$	10 bits

the communication throughput and radar-sensing performance are analyzed in this section. Experimental measurements were performed on rural farmland to avoid interference from other RF transmitters since the measurements are performed in the 2.4 GHz industrial, scientific, and medical (ISM) band. Moreover, the open field environment enabled us to perform LOS experiments, which is generally desired for radar measurements.

Two synchronised FMCW processing chains were implemented in the ARESTOR node to provide for the V- and H-pols channels. The communications receiving node is based on an ES mode in ARESTOR which gathers data at a selected rate, decimating the data as necessary, and saving the results to long term storage for off-line processing. Again two separate processing chains were implemented for the 2-pol capture. The longer term aim is for the signal processing for the communications payload to be carried out within the platform in real-time. This article represents the first published results of the use of the ARESTOR platform for joint radar and communications applications.

The proposed DFRC system is designed to operate in the 2.4 GHz ISM band, accordingly, the generated waveforms must stay within this ISM band, i.e., between 2400 and 2483.5 MHz [41]. Moreover, the minimum and maximum bandwidths of the transmitted radar chirps are determined as 40 and 55 MHz, respectively. Therefore, the number of waveforms that can be transmitted in each polarization are restricted by the center frequency spacing (Δf) and bandwidth spacing (ΔB) due to these frequency spectrum limitations.

Table III presents example waveform bandwidth spacing, center frequency spacing and channel (dual or single) combinations and resulting constellation size (N_{cons}) and the corresponding number of bits (N_{bits}) that can be transmitted within in each radar chirp. During measurements, $\{\Delta B = 5$ MHz, $\Delta f = 5$ MHz$\}$ and $\{\Delta B = 2$ MHz, $\Delta f = 2$ MHz$\}$ modes for dual channel system; and $\{\Delta B = 2$MHz, $\Delta f = 2$ MHz$\}$ and $\{\Delta B = 1$ MHz, $\Delta f = 2$ MHz$\}$ modes for single-channel system are experimentally performed and measured. Other modes given in Table III require larger RAM than is available in ARESTOR to store the entire set of chirp combinations as the entire symbol-set should be stored for V- and H-pols, thus they were not used in experiments. After verifying the simulations by experimental measurements for the aforementioned modes, other modes are realized in simulations. Table III indicates that enabling the dual channel mode provides nearly a 50% increase in the number of bits that can be transmitted using the same bandwidth and center frequency separations (i.e., 9 bits versus 13 bits for $\Delta B = 2$ MHz and $\Delta f = 2$ MHz case). Only the dual channel receiver model presented in Fig. 3(b) is used in simulations and measurements as the performance of the single-channel receiver is limited and it cannot be used to receive the simultaneously transmitted chirps in V- and H-pols.

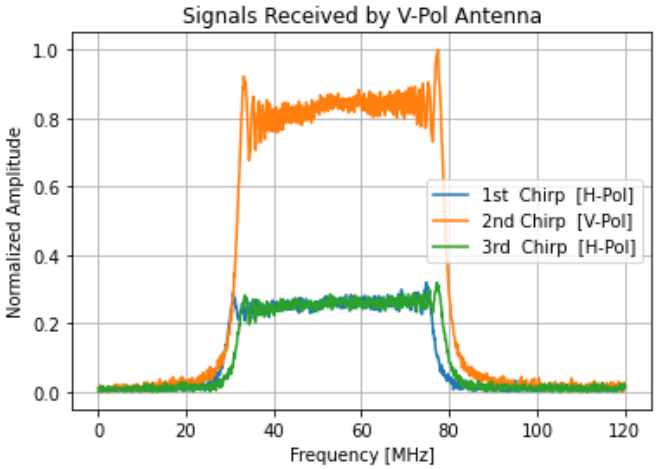

(a)

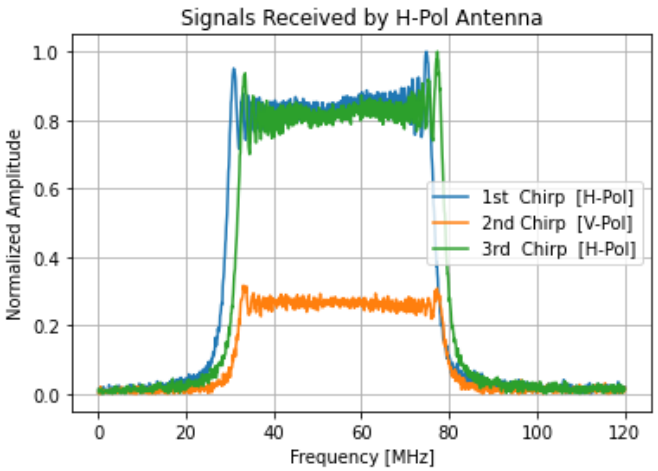

(b)

Fig. 6. Example received signals at H- and V-pols communication antennas when three chirps are transmitted by the radar in either H-pol or V-pol. (a) V-pol receiver. (b) H-pol receiver.

Fig. 6 illustrates the example signals received at V- and H-pols communication antennas when three different index-modulated chirps are transmitted by the dual-polarized radar antenna, i.e., first, second, and third chirps. In this example, the first and third chirps are transmitted by the H-pol DFRC antenna while the second chirp is transmitted by the V-pol DFRC antenna. The signals received at communication V- and H-pols antennas are clearly observed and their center frequency and bandwidth can be determined by the proposed receiver architectures. It can be seen that there is some leakage between the polarizations such that V-pol or H-pol signals are also received by the cross-polarized antennas. This is expected as the cross-polarization isolation of any real antenna is not perfect and there might also be polarization misalignment

between the transmit and receive antennas, resulting in some level of cross-polarization leakage. This polarization leakage is also considered in simulations using the channel model given by (12) and (13).

V. Simulation and Experimental Results

In this section, the communication data rate and radar sensing performance of the proposed DFRC system have been evaluated via simulations and real-time over-the-air experimental measurements performed using the ARESTOR platform [33]. During measurements, ARESTOR platform used for radar sensing performed direct digitization of RF signals, digitally mixing down to baseband and correlating the transmitted and received baseband signals to produce the beat signals. Therefore, only range processing and visualization of the radar images are performed off-line through the stored measurement data. For the communications part, ARESTOR platform performed direct digitization of the received signals and stored the down converted baseband signals at the communication node. The maximum-likelihood estimators and decoding of the communications data are performed offline by a computer using the stored data. Note that it is also possible to implement all digital signal processing on ARESTOR platforms, and this will be investigated in a future study. Measurements provided consistent results with simulations and verified the communication and radar sensing performance of the proposed system.

The performance of the proposed DFRC platform has been evaluated by simulations and experimental measurements performed in the scenario shown in Fig. 5 on a farmland to avoid possible interference from other devices operating in the 2.4 GHz ISM band. Fig. 7 illustrates the measured and simulated throughput of the received communication data. These results have shown that the dual channel system provided a higher data rate and it can also operate in lower SNR per channel compared to the single-channel system. This is mainly due to simultaneously transmitting in both polarizations, even though we transmit with the same power per channel, the overall power consumption, and hence the combined SNR of both channels at the communication receiver are higher since both channels are continuously transmitting. Because, the single channel system transmits chirps in either V-pol, H-pol, or both polarizations, therefore, it does not utilize both channels all time. Experimental measurements and simulations results are in good agreement and they have proved that the proposed DFRC architecture can work even with -10 dB SNR at the communication receiver. This level of SNR performance is due to the extra gain obtained by taking the FFT of the chirps over multiple samples acquired by the ADCs for each chirp before the maximum-likelihood estimator as shown in Fig. 3. This FFT processing gain improves the communication symbol estimation performance by suppressing the random noise [42]. This provides a significant improvement compared to the previous studies such as [23], where higher SNR is required for communication.

Decreasing the chirp duration (i.e., PRI) allows the DFRC system to achieve higher throughput as shown in Fig. 7, however, this is at the expense of sacrificing some degree of

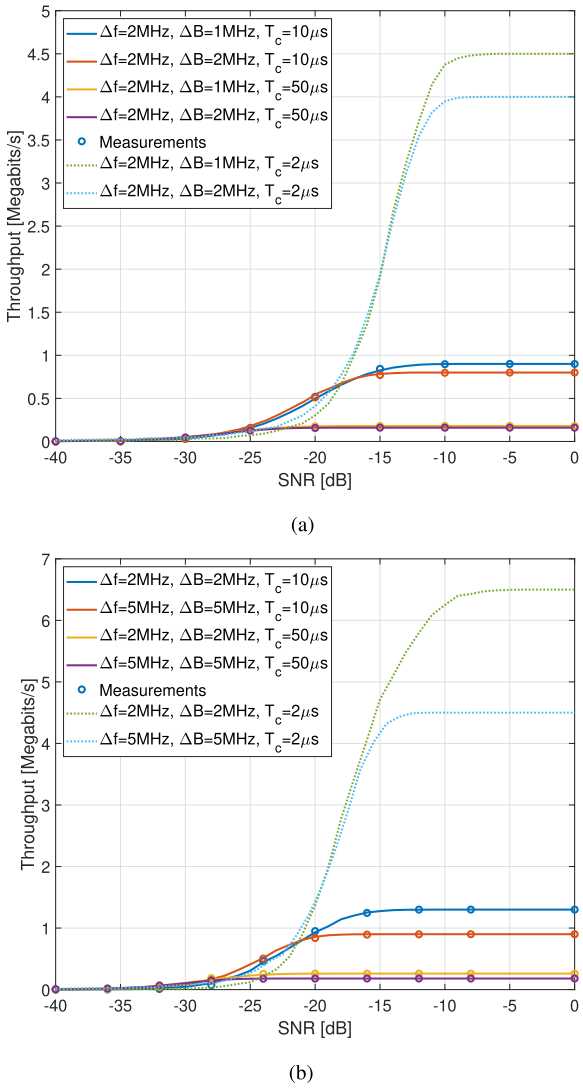

Fig. 7. Measured and simulated throughput of single RF and ADC channel and dual RF and ADC channel radar and communication systems. (a) Single RF and ADC channel system. (b) Dual RF and ADC channel system.

radar performance as observed in Figs. 8 and 9. Fig. 8 presents the radar range image of the static and moving targets from V and H polarized antennas from experimental measurements, where the chirp duration is $T_c = 100$ μs. Both targets are clearly observed although there are some fluctuations that are mainly caused by the varying bandwidth of the FMCW chirps. Note that the target is detected in both polarizations, resulting in obtaining more information about the target, such as some target features might be more visible in one of the polarizations. Fig. 9 shows example radar range images obtained from V polarized antenna with $T_c = 10$ μs and $T_c = 50$ μs chirp durations, respectively. The H-pol radar images are not given here for the sake of brevity. It is seen that when $T_c = 50$ μs both static and moving targets can be detected and their ranges can be estimated. However, when $T_c = 10$ μs, the shorter range static target is still clearly detectable, but the detection of the moving target becomes more challenging as it increases in range. Shorter chirp lengths result in reduced SNR as well as impacting the maximum radar range in FMCW radar systems. The bandwidth of the decimated de-ramped signal in the current ARESTOR implementation limits the operational

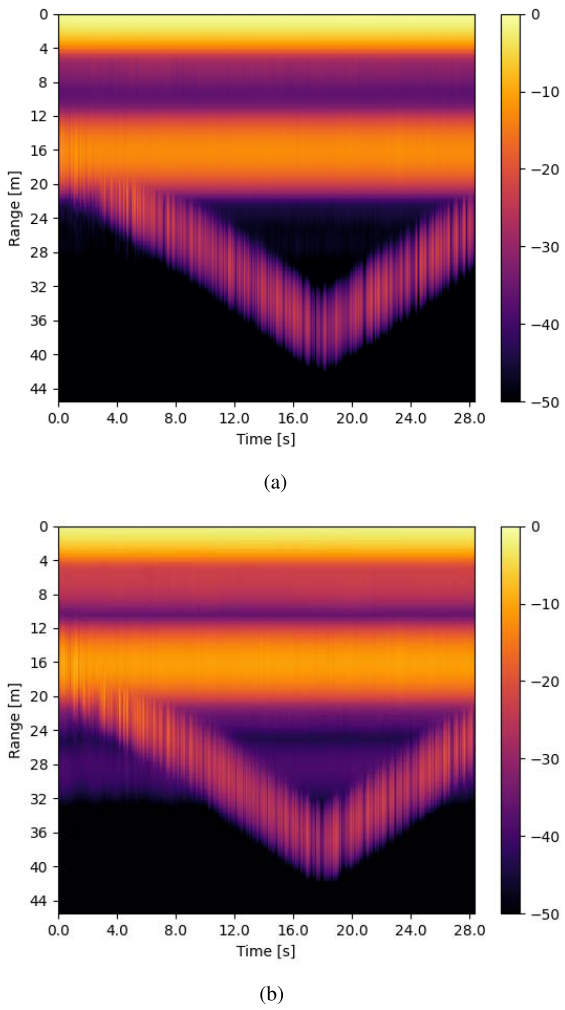

Fig. 8. V- and H-pols radar range measurement images with $T_c = 100$ μs. (a) V-pol radar image. (b) H-pol radar image.

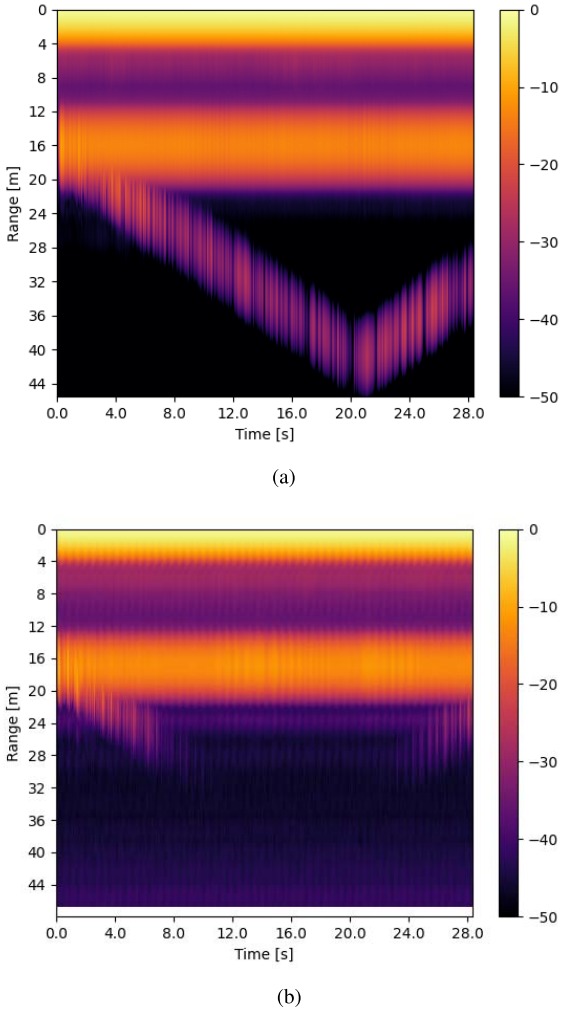

Fig. 9. V-pol radar range measurement images with $T_c = 50$ μs and $T_c = 10$ μs. (a) V-pol radar image with $T_c = 50$ μs. (b) V-pol radar image with $T_c = 10$ μs.

range of the radar with $T_c = 10$ μs to less than 30 m. This range could be increased by changing the characteristics of the decimation filters. This indicates the trade-off between a higher data rate (short chirps) versus higher target SNR (long chirps) and maximum detection range.

These simulation and measurement results have shown a good agreement and give an insight into the expected performance of the proposed DFRC system. Moreover, measurements also enabled us to experimentally evaluate the radar sensing performance. CRLB on the range of the target is analyzed to provide an insightful understanding of the radar performance of the DFRC system. Fig. 10 shows the CRLB on the range of the single-channel DFRC, dual channel DFRC and radar-only scenarios. In the DFRC scenarios, transmitted chirps with bandwidths varying between 40 and 55 MHz were used, as shown in Table III. In the radar-only case chirps with a fixed bandwidth of 50 MHz were used. Due to varying bandwidth, the CRLB on the range of the DFRC scenarios vary, therefore mean values of 10 000 chirps are presented here. It can be seen that the radar-only case reaches a lower CRLB, hence a better range estimation, but the dual channel DFRC can also reach a similar range estimation accuracy. The range estimation accuracy of the single-channel DFRC is worse due to having null chirps during the transmission depending on

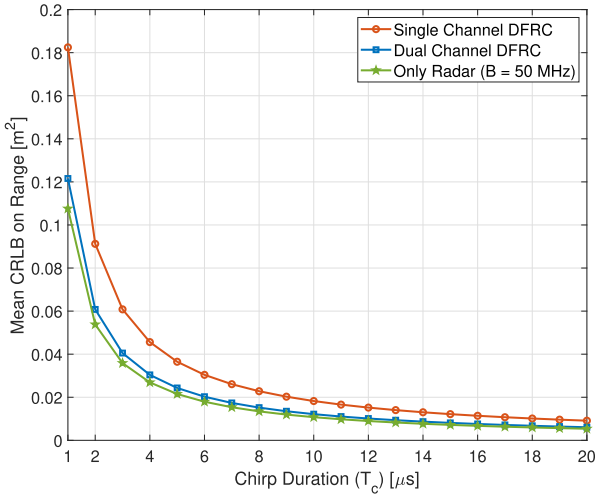

Fig. 10. CRLB on range as a function of chirp duration for DFRC and radar-only cases.

the communication data modulation. Therefore, considering that the communication throughput of the dual-channel DFRC system is also higher than the single-channel system, both radar and communication performance of the dual-channel system is better than the single-channel mode. On the other

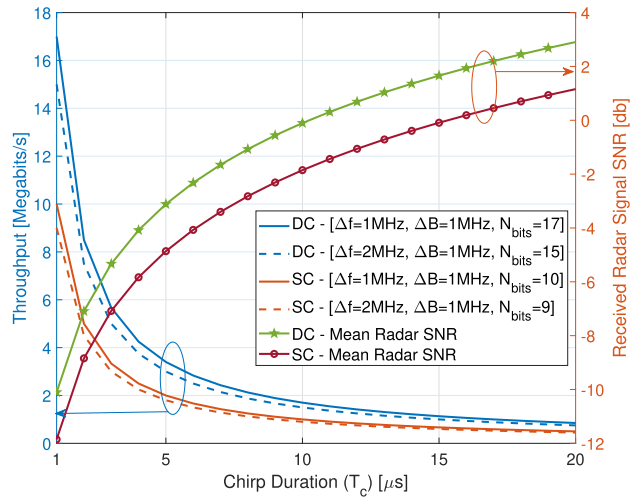

Fig. 11. Radar return SNR and communication throughput as a function of chirp duration. DC represents dual channel while SC represents single channel.

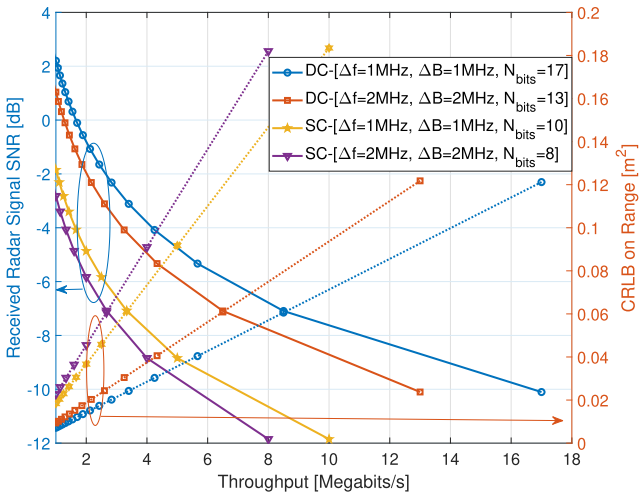

Fig. 12. Trade-off between the maximum throughput, CRLB on range and radar return SNR. (DC represents dual channel while SC represents single channel in the legend).

hand, the advantages of the single-channel system are its lower hardware and computational complexities and also lower power consumption.

Moreover, we also analyzed the direct trade-off between the radar sensing performance and communication throughput in Figs. 11 and 12. Fig. 11 illustrates that chirp duration results in a trade-off between the communication throughput and the radar SNR. Shorter chirp duration enables the DFRC system to transmit data at higher rates while it causes a decrease in the radar SNR. However, this trade-off does not consider integrating multiple chirps, which is expected to improve the radar sensing performance when shorter chirps are employed by integrating multiple of them for radar sensing. This could be investigated in future studies. Depending on the application, a single suitable chirp duration can be chosen to satisfy the radar and communication requirements of the application. For instance, if the DFRC system aims to detect only high SNR targets, then a short chirp duration can be selected to improve the communication throughput while satisfying the radar detection performance, or vice versa. Moreover, the DFRC system can be designed to adaptively operate such that it can continuously adjust the waveform parameters based on the previous sensing information it acquired about the environment and communication users. Fig. 12 shows the relation between the CRLB on the range, throughput and received radar SNR of the DFRC system with different configurations. It clearly shows that selecting a narrower bandwidth and center frequency spacing allows the DFRC system to achieve a better trade-off between communication and radar sensing performance. However, this may also lead to a much larger constellation size, and hence a higher computational complexity of the ML estimators that are utilized to demodulate the received communication data. The dual channel system achieves a better trade-off than the single-channel system in all scenarios simulated or experimentally measured in this study since it simultaneously utilizes both antenna channels to transmit independent chirps.

VI. Conclusion

This study has proposed an IM-based low hardware complexity FMCW DFRC system and evaluated its communication throughput and radar sensing performance by both simulations and experimental measurements. Utilizing dual-polarization antennas and employing bandwidth and center frequency of the chirps as indexes, communications throughputs of up to 17 Mb/s can be achieved. This study has also experimentally demonstrated the trade-off between the communication and radar performance caused by selecting different chirp parameters. Future research may look to investigate and mitigate the impact of the varying chirp parameters and chirp duration on the radar performance. The objective of this would be to correct any undesired radar signal processing effects from the waveform modulations as well as decouple or relax the trade-off between the communication throughput and radar sensing performance.

Acknowledgment

The authors would like to thank the Defense and Security Accelerator (DASA) for supporting this research, and the Air Force Office of Scientific Research and the PETRAS National Centre of Excellence for IoT Systems Cybersecurity for supporting the development of the ARESTOR platform. They would also like to thank Dilan Dhulashia and Piers Beasley for their help with field trials and measurements.

References

[1] F. Liu, C. Masouros, A. P. Petropulu, H. Griffiths, and L. Hanzo, "Joint radar and communication design: Applications, state-of-the-art, and the road ahead," *IEEE Trans. Commun.*, vol. 68, no. 6, pp. 3834–3862, Jun. 2020.

[2] F. Liu, C. Masouros, A. Li, H. Sun, and L. Hanzo, "MU-MIMO communications with MIMO radar: From co-existence to joint transmission," *IEEE Trans. Wireless Commun.*, vol. 17, no. 4, pp. 2755–2770, Apr. 2018.

[3] F. Dong, W. Wang, Z. Hu, and T. Hui, "Low-complexity beamformer design for joint radar and communications systems," *IEEE Commun. Lett.*, vol. 25, no. 1, pp. 259–263, Jan. 2021.

[4] M. Temiz, E. Alsusa, and M. W. Baidas, "Optimized precoders for massive MIMO OFDM dual radar-communication systems," *IEEE Trans. Commun.*, vol. 69, no. 7, pp. 4781–4794, Jul. 2021.

[5] H. Deng and B. Himed, "Interference mitigation processing for spectrum-sharing between radar and wireless communications systems," *IEEE Trans. Aerosp. Electron. Syst.*, vol. 49, no. 3, pp. 1911–1919, Jul. 2013.

[6] C. Aydogdu, M. F. Keskin, N. Garcia, H. Wymeersch, and D. W. Bliss, "RadChat: Spectrum sharing for automotive radar interference mitigation," *IEEE Trans. Intell. Transp. Syst.*, vol. 22, no. 1, pp. 416–429, Jan. 2021.
[7] J. A. Zhang et al., "An overview of signal processing techniques for joint communication and radar sensing," *IEEE J. Sel. Topics Signal Process.*, vol. 15, no. 6, pp. 1295–1315, Nov. 2021.
[8] F. Liu et al., "Integrated sensing and communications: Toward dual-functional wireless networks for 6G and beyond," *IEEE J. Sel. Areas Commun.*, vol. 40, no. 6, pp. 1728–1767, Jun. 2022.
[9] S. D. Blunt, P. Yatham, and J. Stiles, "Intrapulse radar-embedded communications," *IEEE Trans. Aerosp. Electron. Syst.*, vol. 46, no. 3, pp. 1185–1200, Jul. 2010.
[10] S. D. Blunt, J. G. Metcalf, C. R. Biggs, and E. Perrins, "Performance characteristics and metrics for intra-pulse radar-embedded communication," *IEEE J. Sel. Areas Commun.*, vol. 29, no. 10, pp. 2057–2066, Dec. 2011.
[11] Z. Geng, R. Xu, H. Deng, and B. Himed, "Fusion of radar sensing and wireless communications by embedding communication signals into the radar transmit waveform," *IET Radar, Sonar Navigat.*, vol. 12, no. 6, pp. 632–640, Jun. 2018.
[12] C. Sturm and W. Wiesbeck, "Waveform design and signal processing aspects for fusion of wireless communications and radar sensing," *Proc. IEEE*, vol. 99, no. 7, pp. 1236–1259, Jul. 2011.
[13] C. B. Barneto et al., "Full-duplex OFDM radar with LTE and 5G NR waveforms: Challenges, solutions, and measurements," *IEEE Trans. Microw. Theory Techn.*, vol. 67, no. 10, pp. 4042–4054, Jun. 2019.
[14] Y. Li, X. Wang, and Z. Ding, "Multi-target position and velocity estimation using OFDM communication signals," *IEEE Trans. Commun.*, vol. 68, no. 2, pp. 1160–1174, Feb. 2020.
[15] S. H. Dokhanchi, M. R. B. Shankar, Y. A. Nijsure, T. Stifter, S. Sedighi, and B. Ottersten, "Joint automotive radar-communications waveform design," in *Proc. IEEE 28th Annu. Int. Symp. Pers., Indoor, Mobile Radio Commun. (PIMRC)*, Oct. 2017, pp. 1–7.
[16] P. Kumari, S. A. Vorobyov, and R. W. Heath Jr., "Adaptive virtual waveform design for millimeter-wave joint communication-radar," *IEEE Trans. Signal Process.*, vol. 68, pp. 715–730, 2019.
[17] S. H. Dokhanchi, B. Shankar, M. Alaee-Kerahroodi, and B. Ottersten, "Adaptive waveform design for automotive joint radar-communication systems," *IEEE Trans. Veh. Technol.*, vol. 70, no. 5, pp. 4273–4290, May 2021.
[18] E. Basar, M. Wen, R. Mesleh, M. Di Renzo, Y. Xiao, and H. Haas, "Index modulation techniques for next-generation wireless networks," *IEEE Access*, vol. 5, pp. 16693–16746, 2017.
[19] T. Mao, Q. Wang, Z. Wang, and S. Chen, "Novel index modulation techniques: A survey," *IEEE Commun. Surveys Tuts.*, vol. 21, no. 1, pp. 315–348, 1st Quart., 2018.
[20] X. Wang, A. Hassanien, and M. G. Amin, "Dual-function MIMO radar communications system design via sparse array optimization," *IEEE Trans. Aerosp. Electron. Syst.*, vol. 55, no. 3, pp. 1213–1226, Jun. 2019.
[21] T. Huang, N. Shlezinger, X. Xu, Y. Liu, and Y. C. Eldar, "MAJoRCom: A dual-function radar communication system using index modulation," *IEEE Trans. Signal Process.*, vol. 68, pp. 3423–3438, 2020.
[22] A. Sahin, S. S. M. Hoque, and C.-Y. Chen, "Index modulation with circularly-shifted chirps for dual-function radar and communications," *IEEE Trans. Wireless Commun.*, vol. 21, no. 5, pp. 2938–2952, May 2021.
[23] D. Ma, N. Shlezinger, T. Huang, Y. Liu, and Y. Eldar, "FRaC: FMCW-based joint radar-communications system via index modulation," *IEEE J. Sel. Topics Signal Process.*, vol. 15, no. 6, pp. 1348–1364, Nov. 2021.
[24] L. G. de Oliveira, B. Nuss, M. B. Alabd, A. Diewald, M. Pauli, and T. Zwick, "Joint radar-communication systems: Modulation schemes and system design," *IEEE Trans. Microw. Theory Techn.*, vol. 70, no. 3, pp. 1521–1551, Mar. 2022.
[25] D. Ma et al., "Spatial modulation for joint radar-communications systems: Design, analysis, and hardware prototype," *IEEE Trans. Veh. Technol.*, vol. 70, no. 3, pp. 2283–2298, Mar. 2021.
[26] G. Huang, Y. Ding, S. Ouyang, and V. Fusco, "Index modulation for OFDM RadCom systems," *J. Eng.*, vol. 2021, no. 2, pp. 61–72, Feb. 2021.
[27] K. Wu, J. A. Zhang, X. Huang, and Y. J. Guo, "Integrating secure communications into frequency hopping MIMO radar with improved data rate," *IEEE Trans. Wireless Commun.*, vol. 21, no. 7, pp. 5392–5405, Jul. 2022.
[28] K. Wu, J. A. Zhang, X. Huang, Y. J. Guo, and R. W. Heath Jr., "Waveform design and accurate channel estimation for frequency-hopping MIMO radar-based communications," *IEEE Trans. Commun.*, vol. 69, no. 2, pp. 1244–1258, Feb. 2021.
[29] W. Baxter, E. Aboutanios, and A. Hassanien, "Joint radar and communications for frequency-hopped MIMO systems," *IEEE Trans. Signal Process.*, vol. 70, pp. 729–742, 2022.
[30] K. Wu, J. A. Zhang, X. Huang, and Y. J. Guo, "Frequency-hopping MIMO radar-based communications: An overview," *IEEE Aerosp. Electron. Syst. Mag.*, vol. 37, no. 4, pp. 42–54, Apr. 2022.
[31] M. Conti, C. Moscardini, and A. Capria, "Dual-polarization DVB-T passive radar: Experimental results," in *Proc. IEEE Radar Conf. (RadarConf)*, May 2016, pp. 1–5.
[32] Y.-J. Kim, G. Noh, H. L. Lee, and S. Yu, "Dual-polarized multi-channel 24 GHz radar sensor antenna for high channel-to-channel isolation," *Sensors*, vol. 20, no. 18, p. 5233, Sep. 2020.
[33] N. Peters, C. Horne, and M. A. Ritchie, "ARESTOR: A multi-role RF sensor based on the Xilinx RFSoC," in *Proc. 18th Eur. Radar Conf. (EuRAD)*, Apr. 2022, pp. 102–105.
[34] H. D. Griffiths, "New ideas in FM radar," *Electron. Commun. Eng. J.*, vol. 2, no. 5, p. 185, 1990.
[35] A. G. Stove, "Linear FMCW radar techniques," *IEE Proc. F, Radar Signal Process.*, vol. 139, no. 5, p. 343, 1992, doi: 10.1049/ip-f-2.1992.0048.
[36] M. Ritchie, N. Peters, and C. Horne, "Joint active passive sensing using a radio frequency system-on-a-chip based sensor," in *Proc. 23rd Int. Radar Symp. (IRS)*, Sep. 2022, pp. 130–135.
[37] P. Wang, D. Millar, K. Parsons, R. Ma, and P. V. Orlik, "Range accuracy analysis for FMCW systems with source nonlinearity," in *IEEE MTT-S Int. Microw. Symp. Dig.*, Apr. 2019, pp. 1–5.
[38] S. Scherr, S. Ayhan, M. Pauli, and T. Zwick, "Accuracy limits of a K-band FMCW radar with phase evaluation," in *Proc. 9th Eur. Radar Conf.*, Oct. 2012, pp. 246–249.
[39] Xilinx. *Zynq UltraScale+ RFSoC*. Accessed: Aug. 22, 2022. [Online]. Available: https://www.xilinx.com/products/silicon-devices/soc/rfsoc.html
[40] Xilinx. *ZCU111 Evaluation Kit*. [Online]. Available: https://www.xilinx.com/products/boards-and-kits/zcu111.html
[41] *U.K. Radio Interface Requirement for Wideband Transmission Systems Operating in the 2.4 GHz ISM Band*, Ofcom, London, U.K., Jan. 2018.
[42] S. Rapuano and F. J. Harris, "An introduction to FFT and time domain windows," *IEEE Instrum. Meas. Mag.*, vol. 10, no. 6, pp. 32–44, Dec. 2007.

Murat Temiz (Member, IEEE) received the M.Sc. degree in electrical and electronics engineering from the TOBB University of Economics and Technology, Ankara, Turkey, in 2013, and the Ph.D. degree in electrical and electronic engineering from the University of Manchester, Manchester, U.K., in 2020.

His current research interests are massive MIMO communication systems, dual-function radar and communication systems, multistatic and passive radar networks, and applications of machine learning techniques and their applications in integrated sensing and communication systems.

Colin Horne received the B.Sc.(Eng.) degree in computer systems and electronics from King's College London, London, U.K., in 1982, and the Ph.D. degree in electronic and electrical engineering from University College London (UCL), London, in 2020, on the topic of cognitive radar.

He spent several years at the radar Signal Processing Group, Plessey Research Roke Manor, Romsey, U.K., researching land-based and airborne bistatic radar. He subsequently worked on various radar and defense related projects with Marconi Radar, Plessey Radar, Marconi Radar and Control Systems, The Defense Research Agency, and Diehl GmbH, Nurnburg, Germany, before becoming a partner in a small software company providing management and planning tools to manufacturing companies, the company winning a DTI SMART award for innovation.

Dr. Horne is currently a Research Fellow with the Radar Group, UCL, working on various projects applying the Xilinx RFSoC systems to reconfigurable multirole RF sensing.

Nial J. Peters received the B.A./M.Sc. degree in natural sciences (physics) from Cambridge University, Cambridge, U.K., in 2007, the M.Sc. degree in space and plasma physics from the University Center in Svalbard(UNIS), Oslo University (UiO), Oslo, Norway, in 2009, and the Ph.D. degree in volcanology from Cambridge University, in 2014, focusing on instrumentation development and data processing methodologies for monitoring Erebus volcano, Antarctica.

After completing his Ph.D. degree, he undertook a post-doctoral research project split between Cambridge University and University College London (UCL), London, U.K., to design, build, and deploy an FMCW radar system for volcanic monitoring. He is currently a full-time Research Fellow at UCL, where he works on a range of radar-related projects including target classification using micro-Doppler, spectrum-survey for the IoT devices, and multirole RF systems based on Xilinx RFSoC hardware.

Matthew A. Ritchie (Senior Member, IEEE) received the M.Sc. degree in physics from the University of Nottingham, Nottingham, U.K., in 2008, and the Eng.D. degree from University College London (UCL), London, U.K., in association with Thales U.K., in 2013.

He then worked as a Post-Doctoral Research Associate focusing on machine learning applied to multistatic radar for micro-Doppler classification. In 2017, he took a Senior Radar Scientist position at the Defense Science and Technology Laboratories (DSTL). He is now an Associate Professor at UCL within the Radar Sensing Group and focused on areas including multistatic radar, passive radar, micro-Doppler, and multirole RF sensor hardware.

Dr. Ritchie was awarded the 2017 IET RSN Best Paper Award as well as the Bob Hill Award at the 2015 IEEE International Radar Conference. He is currently serves as the Chair for the IEEE Aerospace and System Society (AESS) for the U.K. and Ireland, the Subject Editor-in-Chief for the *IET Electronics Letters* journal, and the Head of the U.K. EMSIG Society.

Christos Masouros (Senior Member, IEEE) received the Diploma degree in electrical and computer engineering from the University of Patras, Patras, Greece, in 2004, and the M.Sc. degree in research and the Ph.D. degree in electrical and electronic engineering from The University of Manchester, Manchester, U.K., in 2006 and 2009, respectively.

In 2008, he was a Research Intern at the Philips Research Laboratory, Redhill, U.K. From 2009 to 2010, he was a Research Associate with The University of Manchester, and from 2010 to 2012, he was a Research Fellow with Queen's University Belfast, Belfast, U.K. In 2012, he joined University College London, London, as a Lecturer. He has held a Royal Academy of Engineering Research Fellowship from 2011 to 2016. Since 2019, he has been a Full Professor of signal processing and wireless communications at the Information and Communication Engineering Research Group, Department of Electrical and Electronic Engineering, and affiliated with the Institute for Communications and Connected Systems, University College London. His research interests lie in the field of wireless communications and signal processing with particular focus on green communications, large scale antenna systems, integrated sensing and communications, interference mitigation techniques for MIMO, and multicarrier communications.

Dr. Masouros was a co-recipient of the 2021 IEEE SPS Young Author Best Paper Award. He was a recipient of the Best Paper Awards in the IEEE GLOBECOM 2015 and IEEE WCNC 2019 conferences. He is a Founding Member and the Vice-Chair of the IEEE Emerging Technology Initiative on Integrated Sensing and Communications, the Vice Chair of the IEEE Special Interest Group on Integrated sensing and communications (ISAC), and the Chair of the IEEE Green Communications and Computing Technical Committee, Special Interest Group on Green ISAC. He has been recognized as an Exemplary Editor for the IEEE COMMUNICATIONS LETTERS, and as an Exemplary Reviewer for the IEEE TRANSACTIONS ON COMMUNICATIONS. He is an Editor for IEEE TRANSACTIONS ON WIRELESS COMMUNICATIONS, the IEEE OPEN JOURNAL OF SIGNAL PROCESSING, and Editor-at-Large for IEEE OPEN JOURNAL OF THE COMMUNICATIONS SOCIETY. He has been an Editor for IEEE TRANSACTIONS ON COMMUNICATIONS, IEEE COMMUNICATIONS LETTERS, and a Guest Editor for a number of IEEE JOURNAL ON SELECTED TOPICS IN SIGNAL PROCESSING and IEEE JOURNAL ON SELECTED AREAS IN COMMUNICATIONS issues.